

**Structure optimization effects on the electronic properties of
 $\text{Bi}_2\text{Sr}_2\text{CaCu}_2\text{O}_8$**

V. Bellini* and F. Manghi

*INFM-National Research Center on nanoStructures and bioSystems at Surfaces (S3)
and Dipartimento di Fisica, Università di Modena e Reggio Emilia,
Via Campi 213/A, I-41100 Modena, Italy*

T. Thonhauser

*Department of Physics, The Pennsylvania State
University, University Park, PA 16802, USA*

C. Ambrosch-Draxl

*Institut für Theoretische Physik, Universität Graz,
Universitätsplatz 5, A-8010 Graz, Austria*

(Dated: November 2, 2018)

Abstract

We present detailed first-principles calculations for the normal state electronic properties of the high T_C superconductor $\text{Bi}_2\text{Sr}_2\text{CaCu}_2\text{O}_8$, by means of the linearized augmented plane wave (LAPW) method within the framework of density functional theory (DFT). As a first step, the body centered tetragonal (BCT) cell has been adopted, and optimized regarding its volume, c/a ratio and internal atomic positions by total energy and force minimizations. The full optimization of the BCT cell leads to small but visible changes in the topology of the Fermi surface, rounding the shape of CuO_2 barrels, and causing both the BiO bands, responsible for the pockets near the \bar{M} 2D symmetry point, to dip below the Fermi level. We have then studied the influence of the distortions in the BiO plane observed in nature by means of a $\sqrt{2} \times \sqrt{2}$ orthorhombic cell (AD-ORTH) with $Bbmb$ space group. Contrary to what has been observed for the Bi-2201 compound, we find that for Bi-2212 the distortion does not sensibly shift the BiO bands which retain their metallic character. As a severe test for the considered structures we present Raman-active phonon frequencies ($q = 0$) and eigenvectors calculated within the frozen-phonon approximation. Focussing on the totally symmetric A_g modes, we observe that for a reliable attribution of the peaks observed in Raman experiments, both c - and a -axis vibrations must be taken into account, the latter being activated by the in-plane orthorhombic distortion.

PACS numbers: 74.25.Kc,74.25.Jb,74.72.Hs,71.15.Mb

I. INTRODUCTION

The study of the electronic properties of the high-temperature superconductors (HTSC) has been a major research topic in material physics, since their discoveries in the late eighties.¹ The normal metallic state ($T > T_c$) of such compounds has been itself a matter of controversy due to the anomalous behavior of its resistivity and transport properties, compared to classical metals. These anomalies seem to point to a non Fermi liquid behavior of the normal state low lying excitations, at least in the low doping regime, and to account for it new theories have been necessarily postulated (see Ref. 2 and references therein). It is equally puzzling that many compounds belonging to different families of HTSC cuprates with different chemical components and crystal structures show on the other hand a remarkably similar behavior. It is now generally accepted that the origin of these similarities stems from the CuO_2 planar complex, existent in different form in all the HTSC cuprate families, where the main physics resides and where it is believed that the Cooper pairs form at low temperature. The one-band Hubbard model, where only the strong interactions in the CuO planes are considered, is able to reproduce the flat quasiparticle band with $\text{Cu}_d\text{-O}_p$ character which tends to pin the Fermi level leading to a van Hove singularity near the X point (or \bar{M} depending on the space group). Such a feature has indeed been observed in angular-resolved photoemission (ARPES) experiments.³

Due to the refinement obtained by modern spectrometers, i.e. better ΔE and Δk resolution, very detailed analysis of the Fermi surface topology started to appear in the literature, renewing the interest in studying the electronic properties in the normal and superconducting state. Among the HTSC cuprates, the two layer compound of the bismuth family, i.e. $\text{Bi}_2\text{Sr}_2\text{CaCu}_2\text{O}_8$ (or Bi-2212 in a shorter notation), has been chosen as a prototype for spectroscopic studies, due to the relative ease of characterizing a stable crystalline surface not exposed to segregation or oxygen depletion phenomena.⁴ A large number of studies can be found in the literature (for a recent review see Ref. 5 and reference therein), which investigated the topology of the Fermi surface of Bi-2212 as a function of photon energy, temperature and doping concentration. There are two major complications in the analysis of the Fermi surface topology. The first is the existence of matrix element effects inherent in the photoexcitation process, which was recently clarified by the theoretical work of Bansil, Lindroos, and coworkers,^{6,7} and supplied for a unified picture on the long debated character,

i.e. ‘hole’ or ‘electron’-like, of the Fermi surface. In addition, diffraction experiments on the composition of Bi-2212 indicated the presence of an incommensurate superstructure^{8,9,10} in the Bi-O plane (or Bi-O ‘modulation’), near to a commensurate orthorhombic distorted cell $\sqrt{2} \times 5\sqrt{2}$ with axes at 45° with respect to the in-plane Cu-O bonds. Refined ARPES measurements have shown the existence of such ‘umklapp’ bands produced by zone-folding along the distortion direction, which overlap with the main Fermi sheets at several points of the Brillouin zone.

In order to interpret the experimental data, detailed analysis from first principles are therefore very much needed, which takes into account all the chemical components of the material. The first band structure calculations of Bi-2212^{11,12,13,14} appeared shortly after the discovery of the Bismuth family of HTSC’s. In all cases, the body centered tetragonal structure, or the face centered structure has been adopted to describe the crystal together with the experimental volume and atomic positions; no real structure optimization has been attempted. Some years ago Singh and Pickett¹⁵ investigated the influence of the orthorhombic distortion in the Bi-O plane on the bands near the Fermi level, although they focused the attention on the one CuO_2 plane compound, i.e. Bi-2201. This work clearly shows that the distortion induces some variations in the binding energy of the bands stemming from the BiO plane, and puts forward that similar effects may play a role also in the two and three CuO layers compounds, Bi-2212 and Bi-2223. The displacements from the tetragonal positions have been indicated as a possible cause for the absence of the BiO pockets at the Fermi surface predicted by photoemission³ and, more unambiguously, tunnelling experiments.^{16,17}

In the following we present a refined analysis of the electronic properties of Bi-2212 by means of first-principles density functional techniques. The work is organized as follows. After a brief introduction of the Bi-2212 crystal structure in Sec. II, the method in use and some computational details are presented in Sec. III. The discussion of the results will be addressed in two separate sections: In Sec. IV we will still rely on the BCT cell, optimizing cell parameters and internal atomic positions, while in Sec. V a possible improvement over the tetragonal description in terms of an “averagely-distorted” orthorhombic (AD-ORTH) cell will be presented. The main focus will be on the Fermi surface topology, and generally, on the band structure close to the Fermi level, and, for the first time to our knowledge, on the calculations of the Raman-active phonon frequencies and eigenvalues from first principles.

II. CRYSTAL STRUCTURE: BCT VS. AD-ORTH

Bi-2212 belongs, together with the one layer (Bi-2201) and three layers (Bi-2223) compounds, to the bismuth HTSC cuprate family. The basic unit is composed of two CuO_2 planes per cell (one Cu and two O atoms per plane) separated by Ca ions, and two Bi-O layers separated from each of the CuO complexes by a Sr-O layer. The Bi-O planes have, similarly to the Cu-O chains in the Yttrium family, the role of a ‘charge reservoir’, attracting electrons and therefore doping the CuO_2 planes with holes. When the complex superstructures in the BiO plane observed by diffraction experiments are neglected, the crystal structure of Bi-2212 is well represented by the body centered tetragonal cell (with space group I_4/mmm) shown in Fig. 1(a). The superstructure arises because of the mismatch between the equilibrium Bi-O bond length and the lattice constant imposed by the CuO_2 planar nets. The weak coupling of the two BiO planes has been found to favor the appearance of such distortion, as opposed to the case of the Tl-2212 compound, where the shorter distance between the TlO planes is responsible for its absence. Moreover, the observed superstructure is incommensurate with respect to the Cu-O lattice constant, and is only approximately arranged by a $\sqrt{2} \times 5\sqrt{2}$ orthorhombic cell (see for instance Fig. 1 in Ref. 8). The full account of these distortions represents a severe task even for modern computers, as far as first-principles supercell calculations are involved. We therefore chose a more simplistic approach, considering the average displacements of the atoms from their tetragonal sites. Insets (b) and (c) in Fig. 1 show how the displacements of the O_{Bi} and Bi atoms in the BiO planes, allowed by an orthorhombic $\sqrt{2} \times \sqrt{2}$ cell (with space group $Bbmb$), account for the mean expansion and contraction of the Bi-O bonds. The type of distortion is the same as simulated by Singh and Pickett¹⁵ for the one layer Bi-2201 compound, whereas we stress that for the Bi-2201 crystal the $\sqrt{2} \times \sqrt{2}$ cell itself is the commensurate analogue to the real incommensurate superstructure. Here, it suffices to say that in-plane average displacements of around 0.5 Å (0.14 Å) along the distortion direction are observed for the O_{Bi} (Bi, O_{Sr}) atoms.⁹ More details on the experimental lattice parameters as well as planar and off-plane coordinates of all the atoms in the BCT and AD-ORTH cells will be given in tables later in the paper.

III. METHOD AND COMPUTATIONAL DETAILS

All calculations have been carried out using the full-potential linearized augmented plane-wave (FP-LAPW) method^{18,19} and its recent extension (APW+lo) as implemented in the WIEN2k code.²⁰ The muffin-tin radii inside which the plane waves are augmented by radial functions expanded over spherical harmonics have been chosen to be 1.9 (Ca), 1.9 (Cu), 2.2 (Sr), 2.25 (Bi), and 1.45 (O) Bohr. Exchange and correlation effects are accounted for by the local density approximation (LDA). In the wave function expansion ≈ 2200 (2400) basis functions at the Γ point have been used, while 40 (27) special \mathbf{k} points within the irreducible part of the BZ sufficed for Brillouin-zone (BZ) integrations for the BCT and AD-ORTH structures, respectively. Starting from the experimental parameters we have optimized the volume and c/a ratio for the BCT (and also b/a for the AD-ORTH cell) by minimization of the total energy. At each step the atoms were allowed to relax to their equilibrium positions under the influence of the Hellmann-Feynman forces, a procedure leading to very accurate equilibrium structures. The remanent forces in this case are less than 0.2 mRy/a.u., which is an important ingredient for the estimation of reliable phonon frequencies. A detailed description of the atomic force calculation within the LAPW method is given in Ref. 21. Within the frozen-phonon approach a polynomial fit of calculated atomic-force values is carried out. For the fully symmetric A_g modes this was done for the equilibrium position plus two to four different displacements of each participating atom along the Cartesian axis. Diagonalisation of the dynamical matrix yields the phonon frequencies as well as the normal vectors of the vibrations.

IV. RESULTS FOR THE BCT CELL

A. Structural optimization

Band structure calculations adopting tetragonal (or almost tetragonal) body centered or face centered cells for the description of the Bi-2212 crystal go back to the late eighties,^{11,12,13,22} shortly after the discovery of high temperature superconductivity in doped La_2CuO_4 ¹ and other cuprates. In all cases lattice parameters taken from experiments have been used and no optimization of the volume and atomic coordinates has been attempted. It has been instead demonstrated recently during the study of another HTSC,²³

i.e. $\text{YBa}_2\text{Cu}_3\text{O}_7$, that the optimization of the crystal parameters (volume, c/a ratio, atomic coordinates) within the local density approximation lead to a better agreement with experiments for what concerns the Fermi surface topology and the values of Raman-active phonon frequencies. Starting from the experimental data by Sunshine et al.²⁴ (Exp) we have optimized the volume (Vol-Opt) or both, volume and c/a ratio (Full-Opt) by standard total energies techniques (see Table I). Atoms were allowed to relax to their equilibrium positions at each step of the minimization procedures. The case where internal coordinates are relaxed using the experimental lattice volume and c/a ratio (Atom-Opt) is also given. As evident from Table I the well known LDA underestimation of the volume amounts to more than 10% (theory 202.2 \AA^3 , experiment 226.3 \AA^3), while for YBCO²³ it was around 6% only. The optimized c/a ratio is 2% larger than the experimental one, but its influence on the cohesive energy and the equilibrium positions of the nuclei is small. The band structure for the experimental cell agrees very well with other LAPW results,^{11,12} and will not be given here. Both, the volume reduction and the increase in the c/a ratio results in a squeezing of the Cu-O in-plane bond length; as a net effect, as will be evidenced in the next section, hybridization between CuO_2 and BiO planes through the SrO plane is favored inducing both BiO bands to cross the Fermi level. This is consistent with the results obtained by Szpunar et al. in Ref. 14, who investigated the effect of stress along the c axis by decreasing the c/a ratio up to 12%, and found consistently the opposite trend, i.e. the BiO bands move to lower energies. For what concerns the atomic coordinates within the cell, a relevant change is the sizable increase of the dimpling in the SrO plane (of around 0.3 \AA), while it is only slightly reduced in the CuO_2 and BiO planes. The dimpling of the CuO_2 plane in HTSC has been shown to be connected to the bifurcation of the saddle point near the \bar{M} point,²⁵ and much attention has been devoted to it in the framework of the van Hove scenario.²⁶

B. Fermi surface

Fig. 2 depicts the calculated cross cuts of the Fermi surface with the $k_z = 0$ plane. The dispersion along the direction perpendicular to the plane is very low due to the high 2D character of the layered cuprates. The contour plots have been obtained by associating a sharp Lorentzian to each eigenvalue and summing the contribution at the Fermi level from all the bands at each k-point; the small broadening induced in this way has therefore no

physical origin. The plots are centered around the $X \equiv (\pi/a, \pi/a)$ point, while $\Gamma \equiv (0, 0)$ and $Z \equiv (0, 2\pi/a)$ (or equivalently $(0, \pi/a)$) are at the corners of the squares. Moving from the experimental structure (Fig. 2(a)) to the fully optimized structure (Fig. 2(b)) we observe small but visible changes in the Fermi surface topology. The two main barrels centered at X , arising from the $\text{Cu}_d\text{-O}_p$ bands, giving rise to the well known hole-like Fermi surface, attain a more rounded shape and the splitting (usually indicated as “bilayer splitting”) of the bonding and antibonding parts is generally reduced. Near the \bar{M} point, where the splitting is expected to be larger, the interpretation is complicated by the hybridization with the BiO orbitals, which induces an anticrossing between the bands. Both BiO bands, with antibonding character and $p_{(x,y)}$ symmetry, are found to cross the Fermi level for the optimized structure, giving rise to two distinct intersecting pockets around \bar{M} , which dope the CuO_2 planes with additional holes. The main issue about these pockets is that there is no evidence of them in both, photoemission and tunnelling experiments, which is normally attributed to the incommensurate structural modulation/distortion present in the BiO plane. (We will come back to this issue in Sec. V B.) Bansil, Lindroos and coworkers^{6,7} have shown by means of the KKR method and one-step photoemission theory that matrix elements modulate the intensity of the spectra at the Fermi level differently depending on the wave vector and energy of the incoming photon. Yet, in all their calculations, the potentials were adjusted in an ad-hoc manner in order to shift the BiO bands above the Fermi level. While matrix elements effect and low scattering cross-sections for the bands in the BiO plane might explain their absence in ARPES measurements, tunnelling experiment on the other hand are less criticizable. Notwithstanding, it has been shown recently that filtering effects stemming from the symmetry of the surface’ electronic states are responsible for the observed suppression of the tunnelling conductance in case of a CuO terminated surface²⁷, and therefore a simulation of scanning tunnelling spectra on BiO-plane terminated surfaces might help in the future to clarify this argument. The explicit treatment of correlation effects in the CuO_2 plane beyond the mean-field does not modify this picture leaving the hybridization between Cu and BiO bands unaltered. Work along this line is under way and will be presented in a separate contribution.²⁸

Since photoemission and even more tunnelling experiments probe only the surface layers of a material and since the BiO plane is the natural cleavage plane during sample preparation, one might argue that the surface BiO bands might slightly deviate from the bulk ones.

We have therefore investigated this possibility and simulated the presence of a BiO plane terminated (001) surface. Thereby we used a supercell technique which considers repeated slabs, each composed of two halves of BCT cells embedded in vacuum. The in-plane lattice constant was the one determined in the optimization of the bulk, while the atoms were allowed to relax along the direction perpendicular to the surface. Such relaxations were found to be of limited size, consistent with the highly two-dimensional nature of the compound, but still induced slight changes in the Fermi surface (see Fig. 2(c)). The dimpling in the BiO plane doubles in value (from 0.09 to 0.16 Å) and the BiO bands becomes almost degenerate crossing the Γ - \bar{M} direction at the same point. The CuO barrels move towards the \bar{M} point and the BiO pockets becomes less distinguishable. Overall, the so optimized Fermi surface compares better with ARPES measurement (see for instance Ref. 29,30,31,32,33,34).

C. Raman-active phonons

A rigorous test for the quality of any structural characterization, is the calculation of the phonon frequencies, which, through the dynamical matrix, gives an account on how well the equilibrium positions as well as the bonding between the atoms are described. For the tetragonal cell, 14 Raman active ($q = 0$) modes ($6A_{1g} + 1B_{1g} + 7E_g$) are predicted by the I_4/mmm space group. The A_{1g} modes are symmetric c -axis vibration of Bi, Sr, Cu, O_{Bi} , O_{Sr} and O_{Cu} atoms, the B_{1g} phonon is the out-of-phase motion of the O_{Cu} atoms also along the c -axis, and E_g vibrations are planar ab displacements. The frequencies of the A_{1g} c -axis Raman-active modes and the corresponding eigenvectors, obtained by the frozen phonon approach, are listed in Table II. We start the discussion by saying that while the frequencies of the measured phonon peaks agree well under similar experimental conditions, their assignments have changed sensibly during the last decade and among different groups. Focusing only on the most recent investigations,³⁵ the strongest dispute concerns the origin of the two highest frequencies, i.e. at around 460 and 630 cm^{-1} , which were attributed to the motion of the O_{Bi} and O_{Sr} atoms^{36,37,38,39,40}, respectively, or viceversa.⁴¹ The frequency around 115 and 130-140 cm^{-1} is concordantly believed to stem from Sr and Cu vibrations along the c -axis. On the other hand, fewer investigations focussed onto the low frequency part of the spectrum where the phonons of the heavier atom, i.e. Bi, should appear, and a well resolved peak at around 60 cm^{-1} has been successfully observed.^{42,43,44} Attribution

of the peaks in the Raman spectra have been achieved either by investigating the change in frequencies and/or intensities upon substitution with Y or Pb atoms, or by isotopes,⁴⁰ or by comparing with existent theoretical calculations. For the former type of analysis, the attribution strongly depends on the choice of the atomic site where the substitution is believed to take place. From the theoretical side, lattice dynamics calculations in the framework of the shell model have been performed more than a decade ago⁴⁵ and found the 6 A_{1g} phonons to be placed at 87, 164, 182, 387, 493 and 517 cm^{-1} . A shortcoming of this method is that the choice of the interatomic potentials, which enter the calculations as parameters, is not unique and consequently interactions in the crystal might be not accounted for properly.

As can be inferred from columns 2-7 of Table II, which list the normal vectors of phonons, we attribute the 6 frequencies, in increasing order of eigenvalue, to the main vibrations of Bi, Cu, Sr, O_{Bi} , O_{Cu} and O_{Sr} . While the motion of the three oxygens have a somewhat purer character, the lower vibrations involve the in- and out-of-phase motion of more than one atom. The most striking deviations from the experiments are found for the vibration of the oxygen atom in the BiO plane (233 vs. 460 cm^{-1}), and the opposite assignment of the phonons at 116 and 163 cm^{-1} . Our calculations support those experiments that attribute the frequency at around 630 cm^{-1} to the c -axis vibration of the apical O_{Sr} atom. Reasonable but not satisfactory agreement is found therefore only for the three phonons stemming from the Bi, O_{Cu} and O_{Sr} atoms, which are found to be around 15% weaker than their experimental counterparts.

What might be the reason for this disagreement? Regarding the opposite attribution of the 116 and 163 cm^{-1} phonons, we might say that explicit inclusion of correlation effects beyond the mean field in the Cu d bands are expected to change the bond strength and orbital localization in the CuO_2 plane, and consequently influence the restoring force acting on the Cu and O atoms. On the other hand LDA (or GGA)-frozen phonon calculations have demonstrated in the recent past to be able to reproduce very accurately the measured Raman-active phonons of other correlated superconductors such as YBaCuO^{23} , $\text{La}_{2-x}\text{Ba}_x\text{CuO}_4^{46}$ and $R\text{Ni}_2\text{B}_2\text{C}$ (with $R=\text{Y,Lu}$)⁴⁷, and it is therefore puzzling why only for Bi-2212 correlation effects should play a role. For what concerns the vibration of the O_{Bi} atom, the calculated vibrational frequency is only half of the measured value, a deviation that is too large to be ascribed to the approximation adopted in the method. The inadequacy

of the tetragonal approximation for the structural characterization of Bi-2212 compound seems therefore the only plausible explanation for this large discrepancy. Expansion and contraction of the Bi-O bonds along the distortion direction, induced by the displacement of the atoms from the tetragonal positions, might change the nature of the bonds together with the mutual distances between the atoms and consequently the stiffness of the restoring force. Moreover modes that are forbidden in a tetragonal cell become Raman-active in an orthorhombic one, and for large atomic displacements even the $q = 0$ selection rules may be affected and additional modes may appear. We will investigate this point in Sec. V C.

V. RESULTS FOR THE AD-ORTH CELL

A. Structural optimization

Similarly to what has been done for the BCT cell, we present in Table III, a comparative listing of structural data for the AD-ORTH structure. Now both, the c/a and b/a lattice constant ratios have been optimized in the AD-ORTH structure. In Table III the labels 'Full-Opt', 'Vol-Opt', 'Exp-Opt' have the same meaning as in Table I. Experimental data for the *Bbmb* cell have been taken from Ref. 9. In addition to the z coordinates of the atoms, the x coordinates are given; the origin of the cell is shifted by $(a/2, b/2, -c/4)$ from the one of the BCT cell, while the orthorhombic x and y axis are rotated by 45° with respect to the tetragonal cell and point along the Bi-O bond directions. Compared to the BCT cell, a smaller reduction of the volume is found by LDA (4.2% vs. 10%); the c/a (b/a) ratio increases (decreases) by about 2 (3.4)%. The atomic z -coordinates are generally very similar to the ones in the BCT cell, while only a slight enhancement of the dimpling in SrO plane is found. As depicted in Fig. 1, the average displacements from the tetragonal positions of the Bi and O atoms in the BiO layers induce alternate expanded and contracted Bi-O bond distances along the x direction, which amount to 2.69 ± 0.64 Å and to 2.67 ± 0.55 Å for the experimental and fully optimized structure, respectively. Along the other bond direction, which is now distorted into a zig-zag line, the average bond distances are 2.72 Å and 2.59 Å for the experimental and optimized cell, respectively. Total energy calculations performed with the experimental lattice constants show that the distorted structure is more stable than the tetragonal one; the difference in the total energy amounts to 0.60 eV per

formula unit, similarly to what has been found for the Bi-2201 compound.¹⁵ This is a first clear indication that the tetragonal description is far from being realistic, and, as put forward for the Bi-2201 compound, one should not entirely rely on it when comparing with ARPES or Raman experiments.

B. Band structure and Fermi surface

The large structural distortion in the BiO plane of the one layer bismuth cuprate, i.e. Bi-2201, has been demonstrated¹⁵ to induce a sensible (400 meV) upwards shift of the partially occupied BiO bands that dip below the Fermi level near the \bar{M} point of the tetragonal Brillouin zone. We plot in Fig. 3 the band structure in the vicinity of the Fermi level for Bi-2212 in the BCT (a) and AD-ORTH structure (b), along the $\Gamma - M$ line of the orthorhombic Brillouin zone; The same k-point direction has been chosen for Bi-2201 so that Fig. 3 and Fig. 3 in Ref. 15 are directly comparable. The \bar{M} 2D symmetry point of the tetragonal cell sits in the middle of the $\Gamma - M$ line. Four of the six bands which cross the Fermi level stem from the BiO plane (doubled by the folding) while the other two are the bilayer-split CuO bands mirrored across the zone boundaries due to the $X \rightarrow \Gamma$ folding. In spite of the similarities between the one and two CuO layers compounds discussed above, it can be inferred from Fig. 3 that the distortion in the Bi-2212 does not sensibly move the BiO bands neither it visibly reduces the hybridization with the CuO bands below. The different behavior of Bi-2201 and Bi-2212 might be ascribed to the stronger interactions between the BiO and CuO₂ planes found in latter; the larger overlap between the orbitals is also testified by the larger number of hole-carriers per CuO₂ plane transferred by the BiO plane.

As a result, now there are many more bands that cross the Fermi level enormously complicating the topology of the Fermi surface, as shown in Fig. 4. While multiple CuO barrels have been detected in several experiments and correctly assigned to the scattering of the photoemitted electron from the orthorhombic distorted BiO planes, no clear evidence of neither one nor several BiO pockets have been found. The similarities between the Bi-2201 and Bi-2212 Fermi surfaces, evidenced by ARPES experiments, on the other hand suggest that the broadening of the bands due to the incommensurate and disordered nature of the distortion together with finite energy resolution of the spectrometers might justify why many of the details of the Fermi surface are smeared out and do not result into clear features at

the Fermi level. Moreover, the photoemission cross section from electrons in the BiO plane is also much smaller than for the CuO₂ planes, which might compromise their detection at the Fermi level.

C. Raman-active phonons

In most of the Raman scattering experiments present in the literature the assignment of the phonon modes have been carried out starting from the $I4/mmm$ space group used for the tetragonal cell. But, since more phonon peaks are usually observed in the spectra than what is expected in a tetragonal structure, it is also a common opinion that several other vibrations become Raman active due to the distortion or to folding at the Brillouin zone edge. As for the BCT cell, also for the AD-ORTH cell the Ca atoms are placed at the centers of inversions and associated vibrations are therefore Raman inactive. A group-theoretical analysis within the $Bbmb$ space group of the orthorhombic cell^{48,49} already appeared in the literature. Limiting ourself to the study of the Raman-active phonons, each set of Cu, Sr, Bi, O_{Sr} and O_{Bi} atoms in the cell (with m point group) contributes with $2 A_g + 1 B_{1g} + 1 B_{2g} + 2 B_{3g}$ modes. The two inequivalent sets of O_{Cu} atoms in the CuO₂ plane, having different point groups, i.e. 2, contribute each with $1 A_g + 1 B_{1g} + 2 B_{2g} + 2 B_{3g}$ modes. Focussing only on the vibrations which do not lower the symmetry of the crystal, i.e. A_g , we expect then to find 12 A_g modes, which in a first approximation separate into 7 vibrations along the c -axis and 5 along the a -axis. Among the c -axis vibrations, only one of them was not active in the tetragonal cell, and stems from the out-of-phase vibration of the two (now inequivalent) O_{Cu} atoms in the CuO₂ plane. Note that the out-of-phase vibration of the O_{Cu} ions is much lower in frequency compared to its counterpart in YBCO. The reason for this should be ascribed to the fact that different displacement patterns are involved due to different point symmetries of the ions in the unit cells.

In Table IV the frequencies of all the 12 A_g modes are listed together with the associated eigenvalues. The first thing we notice is that due to the orthorhombic distortion, the c -axis vibration of the O_{Bi} atom strongly couples with the a -axis vibration of the apical O_{Sr} atoms. As a net results the two frequencies appear at 289 and 192 cm⁻¹. Both modes involve also the vibration of Sr along the a -axis. It might be described as a breathing mode in the SrO plane where an enhancement of the orthorhombic distortion arises whenever the O_{Bi} atom

move towards the SrO plane. Only 5 pure in-phase c -axis vibration remains at 597, 367, 163, 104, 47; they all compare closely to the one obtained for the tetragonal cell (see Table II). The two highest modes at 597 and 367 have increased in the range of 10-20 cm^{-1} , while the Cu vibration decreases by the same amount. The vibrational frequencies associated to Bi and Sr are barely affected. The out-of-phase vibration of the oxygen atoms in the CuO_2 plane has a frequency of 210 cm^{-1} . The O_{Bi} c -axis vibrational frequency has moved from 233 cm^{-1} for the BCT cell to 289 cm^{-1} but remains quite far from its experimentally attributed value of 460 cm^{-1} .

In addition to the modes with pure or mixed c -axis character discussed above there are 4 pure a -axis vibrations, as shown in Table IV. a -axis vibrations of the Bi and Sr atoms are found at 106 and 132 cm^{-1} , respectively. Vibrations of the Cu atoms instead results to be much harder, at a frequency of 355 cm^{-1} , three times larger than the corresponding vibration along the c -axis. This large value should not completely surprise considering that it stems from a vibration which compress and expand the Cu-Cu distance along the bond axis. The most interesting finding is the O_{Bi} a -axis mode, which attains a frequency of 424 cm^{-1} , almost twice the value calculated for its c -axis vibration in the tetragonal cell. It is important to recall that all these modes have A_g symmetry and are thus expected to appear in Raman spectra taken under non-crossed polarization geometry such as (zz), (xx) or (yy). In light of these results, it is therefore very tempting to associate the experimental peak around 460 cm^{-1} to the a -axis rather than the c -axis vibration of the O_{Bi} atom. Calculations of Raman spectra under different scattering geometries might be able to address this important issue in the future and allow for a direct comparison with the experimental spectra.

VI. CONCLUSIONS

We have performed extensive first-principles calculations for the electronic structure of the two layer bismuth cuprate superconductor Bi-2212. By means of the APW+lo method we have optimized the crystal structure for both, a body centered tetragonal cell as well as by taking into account the average distortions in the BiO planes by an orthorhombic $\sqrt{2} \times \sqrt{2}$ cell. When the full optimization of the BCT cell is performed, the main two CuO barrels which characterize the Fermi surface attain a more rounded shape and compare better with what has been measured by ARPES experiments. Calculations show how both the BiO

bands at the \bar{M} symmetry point of the Brillouin zone cross the Fermi level for the optimized structure. The results obtained for a BiO terminated (001) surface exhibit some changes in the details of the Fermi surface, yet of small size due to the two-dimensional layered nature of the double perovskite structure. An analysis of the band structure along the $\Gamma - M$ symmetry line of the orthorhombic AD-ORTH cell, shows that the distortion, despite its large size, leaves the metallic character of the BiO plane unmodified and does not sensibly change the hybridization between the BiO and CuO planes. These findings differ from what has been observed by Singh et al.¹⁵ in the one-layer Bi-2201 compound. In agreement with that work, we predict the distorted structure to be more favorable than the tetragonal one by 0.6 eV per formula unit.

We have then presented first-principles calculations of Raman active phonons within the frozen phonon approach for both, the tetragonal and orthorhombic distorted crystal cells. For the BCT cell, we find reasonable agreement with experiments only for the phonons stemming from vibrations of the Bi, O_{Cu} and O_{Sr} atoms, which are, however, still around 15% lower in frequency than their experimental counterparts. We predict the opposite attribution for the two phonons, which have been associated to vibrations of the Sr and Cu atoms, respectively by experiments on Y- or Pb-substituted samples. Even more severe is the disagreement of the O_{Bi} mode, where we predict a value that is only half of what is experimentally attributed. Due to the distortion along one of the BiO bond directions, giving rise to an orthorhombic cell, more vibrations become Raman-active with a total of 12 A_g modes. There are two main effects induced by this distortion. The first is a coupling of the c -axis vibration of O_{Bi} with the in-plane vibrations in the SrO plane. Secondly, several a -axis vibrations appear due to the symmetry lowering. Among them, the one associated to the O_{Bi} atoms exhibits a frequency of 424^{-1} . It is very near to a peak observed in the measured Raman spectra which is generally assigned as the c -axis O_{Bi} vibration. Our results demonstrate clearly that the distortions have a huge effect, and should be taken into account when a study of lattice vibration of Bi2212 is attempted. In spite of this, the final assignment of the phonon frequencies is not yet fully solved, and calculations of Raman spectra under different scattering geometries might be of help in the future.

Acknowledgments

We are grateful to E. Ya. Sherman for fruitful discussions on phonon frequencies. This work was partly funded by MIUR-‘Progetto Giovani Ricercatori’, and benefitted from support by the Austrian Science Fund (FWF, project P13430) and the EU RTN network EX-CITING, contract HPRN-2002-00317. The computer facilities were granted by an INFM project “Iniziativa Trasversale Calcolo Parallelo” at the CINECA supercomputing center.

* Corresponding author: bellini.valerio@unimore.it

- ¹ J. G. Bednorz and K. A. Mueller, *Z. Physik B* **64**, 189 (1986).
- ² P. W. Anderson, *Physica C* **185-189**, 11 (1991).
- ³ D. S. Dessau, Z.-X. Shen, D. M. King, D. S. Marshall, L. W. Lombardo, P. H. Dickinson, A. G. Loeser, J. DiCarlo, C.-H. Park, A. Kapitulnik, et al., *Phys. Rev. Letters* **71**, 2781 (1993).
- ⁴ D. M. Ori, A. Goldoni, U. del Pennino, and F. Parmigiani, *Phys. Rev. B* **52**, 3727 (1995).
- ⁵ A. Damascelli, D. H. Lu, and Z. X. Shen, *J. Electron. Spectrosc. Relat. Phenom.* **117-118**, 165 (2001).
- ⁶ A. Bansil and M. Lindroos, *Phys. Rev. Letters* **83**, 5154 (1999).
- ⁷ M. Lindroos, S. Sahrakorpi, and A. Bansil, *Phys. Rev. B* **65**, 054514 (2002).
- ⁸ A. A. Levin, Yu I. Smolin, and Yu F. Shepelev, *J. Phys.: Condensed Matter* **6**, 3539 (1994).
- ⁹ P. A. Miles, S. J. Kennedy, G. J. McIntyre, G. D. Gu, G. J. Russell, and N. Koshizuka, *Physica C* **294**, 275 (1998).
- ¹⁰ J. Etrillard, P. Bourges, and C. T. Lin, *Phys. Rev. B* **62**, 150 (2000).
- ¹¹ S. Massidda, J. Yu, and A. J. Freeman, *Physica C* **152**, 251 (1988).
- ¹² H. Krakauer and W. E. Pickett, *Phys. Rev. Letters* **60**, 1665 (1988).
- ¹³ M. S. Hybertsen and L. F. Mattheiss, *Phys. Rev. Letters* **60**, 1661 (1988).
- ¹⁴ B. Szpunar and V. H. Smith Jr., *Phys. Rev. B* **45**, 10616 (1992).
- ¹⁵ D. J. Singh and W. E. Pickett, *Phys. Rev. B* **51**, 3128 (1995).
- ¹⁶ M. Tanaka, *Science* **339**, 691 (1989).
- ¹⁷ C. K. Shih, R. M. Feenstra, and G. V. Chandrashekhar, *Phys. Rev. B* **43**, 7913 (1991).
- ¹⁸ O. K. Andersen, *Phys. Rev. B* **12**, 3060 (1975).

- ¹⁹ D. J. Singh, *Planewaves pseudopotentials and the LAPW method* (Kluwer Academic Publishers, 1994).
- ²⁰ P. Blaha, K. Schwarz, G. Madsen, D. Kvasnicka, and J. Luitz, *WIEN2k, An Augmented Plane Wave + Local Orbitals Program for Calculating Crystal Properties*, (Karlheinz Schwarz, Techn. Universität Wien, Austria) (1999), ISBN 3-9501031-1-2.
- ²¹ R. Kouba and C. Ambrosch-Draxl, Phys. Rev. B **56**, 14766 (1997).
- ²² L. Szunyogh, G. Hörmandinger, and P. Weinberger, Phys. Rev. B **43**, 13025 (1991).
- ²³ R. Kouba, C. Ambrosch-Draxl, and B. Zangger, Phys. Rev. B **60**, 9321 (1999).
- ²⁴ S. A. Sunshine, T. Siegrist, L. F. Schneemeyer, D. W. Murphy, R. J. Cava, B. Batlogg, R. B. van Dover, R. M. Fleming, S. H. Glarum, S. Nakahara, et al., Phys. Rev. B **38**, 893 (1988).
- ²⁵ O. K. Andersen, O. Jepsen, A. I. Lichtenstein, and I. I. Mazin, Phys. Rev. B **49**, 4145 (1994).
- ²⁶ R. S. Markiewicz, J. Phys. Chem. Solids **58**, 1179 (1997).
- ²⁷ S. Misra, S. Oh, D. J. Hornbaker, T. DiLuccio, J. N. Eckstein, and A. Yazdani, Phys. Rev. Letters **89**, 087002 (2002).
- ²⁸ V. Bellini, C. A. Rozzi, and F. Manghi, (unpublished).
- ²⁹ P. Aebi, J. Osterwalder, P. Schwaller, L. Schlapbach, M. Shimoda, T. Mochiku, and K. Kadowaki, Phys. Rev. Letters **72**, 2757 (1994).
- ³⁰ P. V. Bogdanov, A. Lanzara, X. J. Zhou, S. A. Kellar, D. L. Feng, E. D. Lu, H. Eisaki, J.-I. Shimoyama, K. Kishio, Z. Hussain, et al., Phys. Rev. B **64**, 180505 (2001).
- ³¹ T. Sato, T. Kamiyama, T. Takahashi, J. Mesot, A. Kaminski, J. C. Campuzano, H. M. Fretwell, T. Takeuchi, H. Ding, I. Chong, et al., Phys. Rev. B **64**, 054502 (2001).
- ³² D. L. Feng, C. Kim, H. Eisaki, D. H. Lu, A. Damascelli, K. M. Shen, F. Ronning, N. P. Armitage, N. Kaneko, M. Greven, et al., Phys. Rev. B **65**, 220501 (2002).
- ³³ A. A. Kordyuk, S. V. Borisenko, M. S. Golden, S. Legner, K. A. Nenkov, M. Knupfer, J. Fink, H. Berger, L. Forró, and R. Follath, Phys. Rev. B **66**, 014502 (2002).
- ³⁴ M. C. Asensio, J. Avila, L. Roca, A. Tejada, G. D. Gu, M. Lindroos, R. S. Markiewicz, and A. Bansil, Phys. Rev. B **67**, 014519 (2003).
- ³⁵ Experiments previous to 1996 disagree with each other on the interpretation of several of the phonon peaks: see, for instance, Tab. I in Ref. 36, and reference therein.
- ³⁶ M. Kakihana, M. Osada, M. Käll, L. Börjesson, H. Mazaki, H. Yasuoka, M. Yashima, and M. Yoshimura, Phys. Rev. B **53**, 11796 (1996).

FIG. 1: (Color online) In (a) half of the primitive unit of the body centered tetragonal (BCT) cell with space group $I4/mmm$ of Bi-2212 is depicted. In (b) and (c) the BiO plane is sketched in absence or presence of the distortion, respectively. The orthorhombic cell is rotated by 45° in the ab plane with respect to tetragonal one.

FIG. 2: (Color online) Fermi surface cross cuts in the k_x - k_y plane ($k_z = 0$) for the BCT cell with (a) experimental and (b) optimized lattice constants and atomic positions (see Tab. I). (c) The same as in (b), but in the presence of a BiO terminated (001) surface, where the atomic positions were further relaxed in order to account for the breaking of the bonds at the surface layer.

- ³⁷ X. H. Chen, K. Q. Ruan, G. G. Qian, S. Y. Li, L. Z. Cao, J. Zou, and C. Y. Xu, Phys. Rev. B **58**, 5868 (1998).
- ³⁸ M. Osada, M. Kakihana, H. Arashi, M. Käll, and L. Börjesson, Phys. Rev. B **59**, 8447 (1999).
- ³⁹ G. V. M. Williams, D. M. Pooke, D. J. Pringle, H. J. Trodahl, J. L. Tallon, J. Quilty, N. Malde, J. L. Macmanus-Driscoll, A. Crossley, and L. F. Cohen, Phys. Rev. B **62**, 1379 (2000).
- ⁴⁰ A. E. Pantoja, D. M. Pooke, H. J. Trodahl, and J. C. Irwin, Phys. Rev. B **58**, 5219 (1998).
- ⁴¹ C. Kendziora, S. B. Qadri, and E. Skelton, Phys. Rev. B **56**, 14717 (1997).
- ⁴² M. Osada, M. Kakihana, K. Mikael, and L. Börjesson, J. Phys. Chem. Solids **59**, 2003 (1998).
- ⁴³ M. Boekholt, G. Güntherodt, and V. V. Moshchalkov, Physica C **192**, 191 (1992).
- ⁴⁴ J. Sapiel, J. Schneck, J. F. Scott, J. C. Tolédano, L. Pierre, J. Chavignon, C. Daguet, J. P. Chaminade, and H. Boyer, Phys. Rev. B **43**, 6259 (1991).
- ⁴⁵ J. Prade, A. D. Kulkarni, F. W. de Wette, U. Schröder, and W. Kress, Phys. Rev. B **39**, 2771 (1989).
- ⁴⁶ T. Thonhauser and C. Ambrosch-Draxl, Phys. Rev. B **67**, 134508 (2003).
- ⁴⁷ P. Ravindran, A. Kjekshus, H. Fjellvåg, P. Puschnig, C. Ambrosch-Draxl, L. Nordström, and B. Johansson, Phys. Rev. B **67**, 104507 (2003).
- ⁴⁸ S. Sugai and M. Sato, Jap. J. Appl. Phys. **28**, L1361 (1989).
- ⁴⁹ R. Liu, M. V. Klein, P. D. Han, and D. A. Payne, Phys. Rev. B **45**, 7392 (1992).

FIG. 3: Band structure of the undistorted (a) and distorted (b) orthorhombic cell along the $\Gamma - M$ direction in the orthorhombic Brillouin zone; the tetragonal \bar{M} point lies in the middle of the $\Gamma - M$ line.

FIG. 4: (Color online) Fermi surface cross cuts in the k_x - k_y plane ($k_z = 0$) for the AD-ORTH structure: the rotated square (dashed line) whose corners are the Γ point in the middle of the two axis compares with the tetragonal Brillouin zones shown in Fig. 2

TABLE I: Lattice parameters and atomic coordinates (in units of lattice constants) for the BCT structure of Bi-2212: columns 1 to 3 refer to different optimization levels (see text for the details), while in the last column the experimental data taken from Ref.24 are listed.

| | Full-Opt | Vol-Opt | Atom-Opt | Exp |
|----------------------------|----------|---------|----------|--------|
| Vol [\AA^3] | 202.2 | 202.2 | 226.3 | 226.3 |
| c/a | 8.258 | 8.065 | 8.065 | 8.065 |
| $\Delta(E)$ [mRy] | -67.4 | -65.1 | 0 | - |
| z_{Cu} | 0.0499 | 0.0498 | 0.0491 | 0.0543 |
| z_{Sr} | 0.1100 | 0.1103 | 0.1058 | 0.1091 |
| z_{Bi} | 0.2008 | 0.2015 | 0.1949 | 0.1989 |
| $z_{\text{O}_{\text{Cu}}}$ | 0.0514 | 0.0513 | 0.0503 | 0.0510 |
| $z_{\text{O}_{\text{Sr}}}$ | 0.1331 | 0.1328 | 0.1296 | 0.1200 |
| $z_{\text{O}_{\text{Bi}}}$ | 0.1991 | 0.2000 | 0.1929 | 0.1980 |

TABLE II: Frequencies ω (in cm^{-1}) and eigenvectors of the 6 A_{1g} c-axis modes in the BCT cell.

| ω | Cu | Sr | Bi | O_{Cu} | O_{Sr} | O_{Bi} |
|----------|--------------|-------------|--------------|--------------|-------------|--------------|
| 576 | 0.03 | 0.02 | -0.27 | -0.19 | 0.94 | 0.09 |
| 356 | 0.05 | 0.27 | 0.05 | -0.94 | -0.19 | 0.03 |
| 233 | 0.00 | -0.03 | 0.21 | -0.06 | 0.14 | -0.96 |
| 163 | -0.33 | 0.87 | -0.27 | 0.22 | -0.03 | -0.10 |
| 116 | -0.92 | -0.23 | 0.25 | -0.12 | 0.07 | 0.08 |
| 50 | -0.17 | -0.34 | -0.86 | -0.11 | -0.24 | -0.21 |

TABLE III: Lattice parameters and atomic coordinates (in unit of lattice constants) for the AD-ORTH structure of Bi-2212: the experimental data are taken from Ref.9

| | Full-Opt | Vol-Opt | Atom-Opt | Exp |
|--------------------------------|----------|------------|------------|------------|
| Vol [\AA^3] | 428.1 | 428.1 | 446.7 | 446.7 |
| c/a | 5.827 | 5.711 | 5.711 | 5.711 |
| b/a | 0.963 | $\simeq 1$ | $\simeq 1$ | $\simeq 1$ |
| $\Delta(E)$ [mRy] | -52.4 | -35.2 | 0 | - |
| z_{Cu} | 0.2019 | 0.2013 | 0.2011 | 0.1978 |
| z_{Sr} | 0.1441 | 0.1435 | 0.1445 | 0.1405 |
| z_{Bi} | 0.0543 | 0.0528 | 0.0542 | 0.0525 |
| $z_{\text{O}_{\text{Cu}}^1}$ | 0.1995 | 0.1991 | 0.1991 | 0.1976 |
| $z_{\text{O}_{\text{Cu}}^2}$ | 0.2006 | 0.2002 | 0.2002 | 0.1994 |
| $z_{\text{O}_{\text{Sr}}}$ | 0.1192 | 0.1192 | 0.1193 | 0.1189 |
| $z_{\text{O}_{\text{Bi}}}$ | 0.0568 | 0.0554 | 0.0571 | 0.0500 |
| x_{Cu} | 0.2497 | 0.2497 | 0.2496 | 0.2506 |
| x_{Sr} | 0.2526 | 0.2524 | 0.2536 | 0.2500 |
| x_{Bi} | 0.2269 | 0.2255 | 0.2202 | 0.2258 |
| $x_{\text{O}_{\text{Cu}}^1}^a$ | 0.0000 | 0.0000 | 0.0000 | 0.0012 |
| $x_{\text{O}_{\text{Cu}}^2}^a$ | 0.5000 | 0.5000 | 0.5000 | 0.4993 |
| $x_{\text{O}_{\text{Sr}}}$ | 0.2666 | 0.2663 | 0.2675 | 0.2750 |
| $x_{\text{O}_{\text{Bi}}}$ | 0.1705 | 0.1726 | 0.1703 | 0.1561 |

^aThe O_{Cu} atoms retain their tetragonal positions in our calculations.

TABLE IV: Frequencies ω (in cm^{-1}) and eigenvectors of the 12 A_g modes in the AD-ORTH cell. The atoms vibrate along the c- and a- axis, as indicated.

| ω | Cu | Cu | Sr | Sr | Bi | Bi | O_{Cu}^1 | O_{Cu}^2 | O_{Sr} | O_{Sr} | O_{Bi} | O_{Bi} |
|----------|-------------|--------------|-------------|--------------|-------------|--------------|-------------|--------------|-------------|--------------|-------------|--------------|
| | c-axis | a-axis | c-axis | a-axis | c-axis | a-axis | c-axis | c-axis | c-axis | a-axis | c-axis | a-axis |
| 597 | 0.02 | 0.00 | 0.02 | 0.00 | -0.25 | -0.02 | -0.09 | -0.10 | 0.95 | 0.12 | 0.05 | 0.04 |
| 424 | 0.00 | 0.00 | -0.03 | 0.01 | 0.00 | -0.21 | 0.04 | 0.03 | 0.05 | -0.06 | -0.01 | -0.97 |
| 367 | -0.09 | -0.28 | -0.19 | -0.03 | -0.02 | -0.01 | 0.67 | 0.63 | 0.12 | 0.08 | -0.08 | 0.06 |
| 356 | 0.02 | -0.95 | 0.06 | -0.10 | 0.01 | 0.00 | -0.12 | -0.27 | -0.04 | 0.03 | 0.01 | -0.02 |
| 289 | -0.01 | -0.06 | 0.02 | 0.09 | -0.22 | 0.16 | 0.02 | 0.12 | 0.00 | -0.65 | 0.69 | 0.00 |
| 210 | -0.02 | 0.10 | 0.00 | 0.09 | -0.09 | 0.00 | 0.65 | -0.62 | -0.08 | 0.26 | 0.31 | -0.02 |
| 192 | -0.03 | 0.04 | 0.21 | -0.45 | -0.22 | -0.14 | -0.19 | 0.27 | -0.15 | 0.55 | 0.49 | -0.03 |
| 163 | -0.30 | -0.01 | 0.88 | 0.17 | -0.17 | 0.06 | 0.13 | 0.07 | -0.01 | -0.07 | -0.20 | -0.03 |
| 132 | -0.07 | 0.10 | 0.06 | -0.86 | 0.08 | 0.15 | 0.18 | -0.17 | 0.08 | -0.33 | -0.19 | -0.01 |
| 106 | -0.41 | 0.01 | -0.07 | -0.04 | 0.02 | -0.86 | -0.01 | -0.08 | 0.01 | -0.20 | 0.03 | 0.20 |
| 104 | 0.84 | 0.00 | 0.22 | -0.04 | -0.22 | -0.37 | 0.14 | 0.03 | -0.05 | -0.14 | -0.11 | 0.09 |
| 47 | 0.16 | 0.00 | 0.28 | 0.01 | 0.86 | -0.08 | 0.06 | 0.07 | 0.21 | 0.02 | 0.29 | 0.02 |

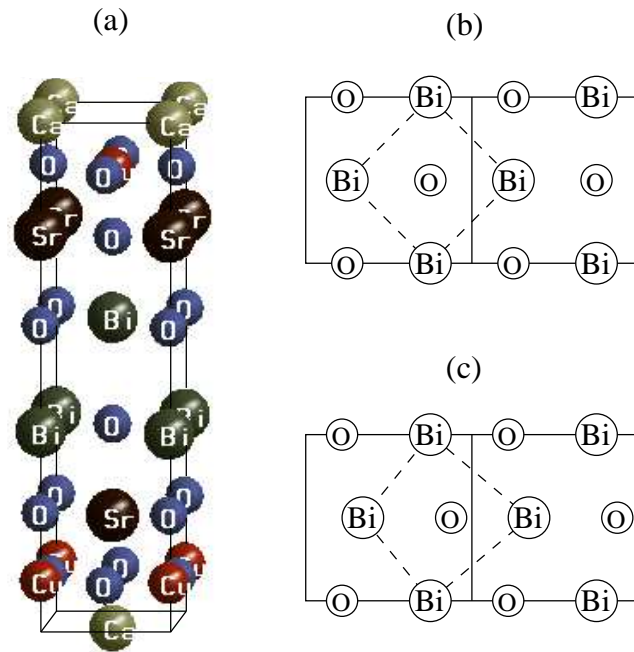


Fig. 1
 Bellini Valerio
 Phys. Rev. B

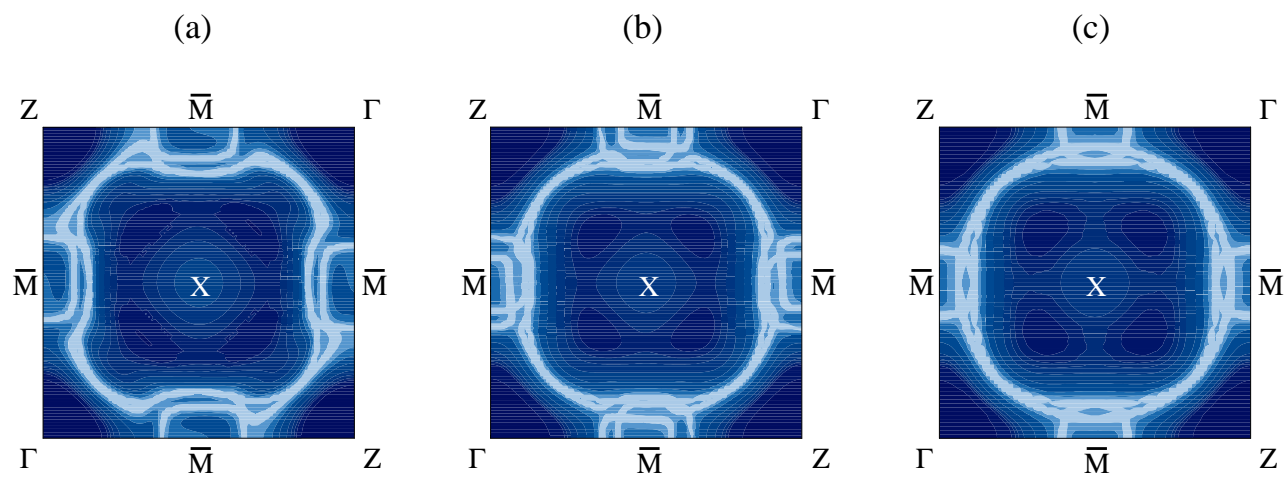


Fig. 2
Bellini Valerio
Phys. Rev. B

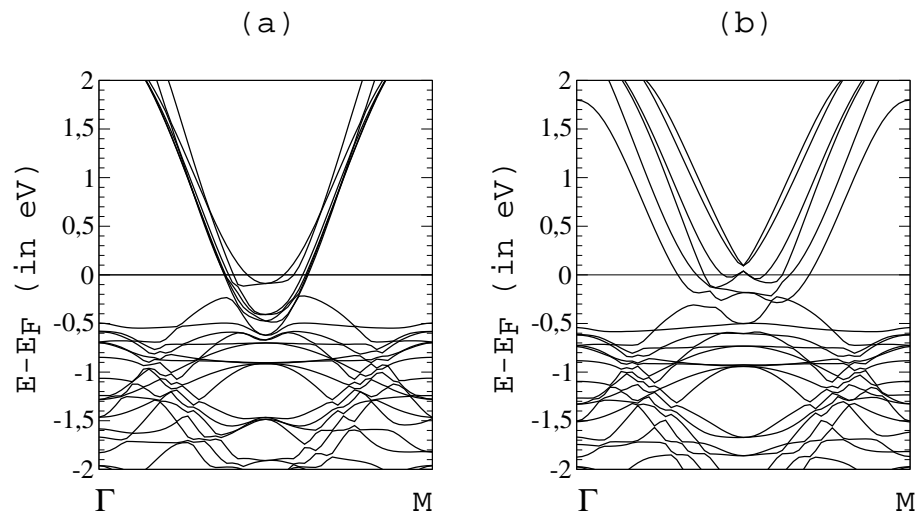


Fig. 3
Bellini Valerio
Phys. Rev. B

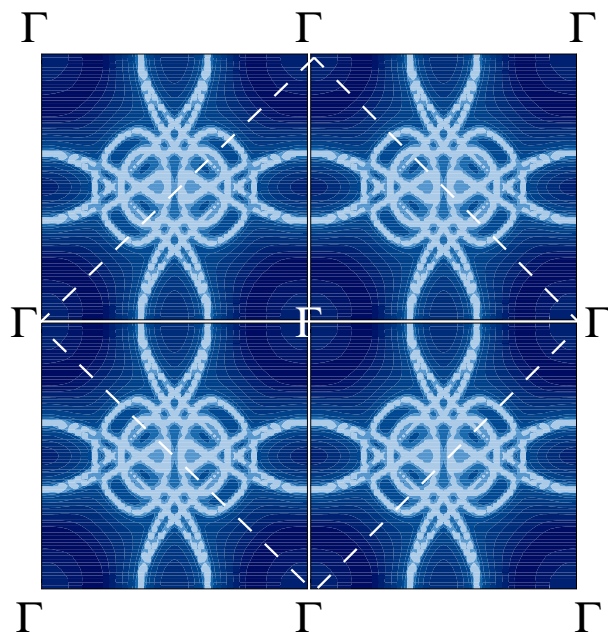


Fig. 4
Bellini Valerio
Phys. Rev. B